

See discussions, stats, and author profiles for this publication at: <https://www.researchgate.net/publication/221362812>

Visibility in bad weather from a single image

Conference Paper in *Proceedings / CVPR, IEEE Computer Society Conference on Computer Vision and Pattern Recognition. IEEE Computer Society Conference on Computer Vision and Pattern Recognition* · June 2008

DOI: 10.1109/CVPR.2008.4587643 · Source: DBLP

CITATIONS

1,320

READS

5,173

1 author:



[Robby T. Tan](#)

Yale-NUS College

104 PUBLICATIONS 4,065 CITATIONS

SEE PROFILE

Visibility in Bad Weather from a Single Image

Robby T. Tan

Imperial College London

Communications and Signal Processing Group *

(formerly at NICTA/The Australian National University)

Abstract

Bad weather, such as fog and haze, can significantly degrade the visibility of a scene. Optically, this is due to the substantial presence of particles in the atmosphere that absorb and scatter light. In computer vision, the absorption and scattering processes are commonly modeled by a linear combination of the direct attenuation and the airlight. Based on this model, a few methods have been proposed, and most of them require multiple input images of a scene, which have either different degrees of polarization or different atmospheric conditions. This requirement is the main drawback of these methods, since in many situations, it is difficult to be fulfilled. To resolve the problem, we introduce an automated method that only requires a single input image. This method is based on two basic observations: first, images with enhanced visibility (or clear-day images) have more contrast than images plagued by bad weather; second, airlight whose variation mainly depends on the distance of objects to the viewer, tends to be smooth. Relying on these two observations, we develop a cost function in the framework of Markov random fields, which can be efficiently optimized by various techniques, such as graph-cuts or belief propagation. The method does not require the geometrical information of the input image, and is applicable for both color and gray images.

1. Introduction

Poor visibility in bad weather is a major problem for many applications of computer vision. Most automatic systems for surveillance, intelligent vehicles, outdoor object recognition, etc., assume that the input images have clear visibility. Unfortunately, this is not always true in many situations, therefore enhancing visibility is an inevitable task.

Optically, poor visibility in bad weather is due to the substantial presence of atmospheric particles that have significant size and distribution in the participating medium. Light from the atmosphere and light reflected from an object are absorbed and scattered by those particles, causing the visibility of a scene to be degraded.

In the literature, a few approaches have been proposed. The first approach is to use polarizing filters (e.g. [10, 11]).

*robby.tan@imperial.ac.uk



Figure 1. Left: an image plagued by fog. Right: the result of enhancing visibility using the method introduced in this paper.

The main idea of this approach is to exploit two or more images of the same scene that have different degrees of polarization (DOP), which are obtained by rotating a polarizing filter attached to the camera. The common drawback of the methods in this approach is that they cannot be applied to dynamic scenes for which the changes are more rapid than the filter rotation in finding the maximum and minimum DOP.

The second approach is to use multiple images taken from bad weather scenes (e.g. [1, 8, 7]). The basic idea of this approach is to exploit the differences of two or more images of the same scene that have different properties of the participating medium. While the methods in this approach can significantly enhance visibility, unfortunately their requirements render them unable to deliver the results immediately (have to wait until the properties of the medium change) for scenes that have never been encountered before. Moreover, like the first approach, they also cannot handle dynamic scenes.

The third approach is to use a single image and demand the approximated 3D geometrical model of the input scene (e.g. [6, 4]). Compared with the previous two approaches, this approach resolves the requirements of multiple images; however, their demand of the approximated 3D geometrical models is problematic, since the structure of the real world (both natural scenes and man-made scenes) are significantly varied. In addition, the method of Narasimhan et al. [6] is not intended to be automatic, it needs user interactions.

To solve the problems, we introduce an automated

method that only requires a single input image. Unlike the existing methods that use a single image, the proposed method does not require the geometrical information of the input image, nor any user interactions. The method is based on two basic observations: first, images with enhanced visibility (or clear-day images) have more contrast than images plagued by bad weather; second, airlight whose variation mainly depends on the distance of objects to the viewer, tends to be smooth. Relying on these two observations, we develop a cost function in the framework of Markov random fields (MRFs), which can be efficiently optimized by various techniques, such as graph-cuts or belief propagation. The method is applicable for both color and gray images.

A brief overview of the method is as follows. Given an input image, we first estimate the atmospheric light, from which we can obtain the light chromaticity. Using the light chromaticity, we remove the light color of the input image. Subsequently, we compute the data cost and smoothness cost for every pixel. The data cost is computed from the contrast of a small patch cropped from the image. The smoothness cost is computed from the difference or distance of the labels of two neighboring pixels, where the labels are identical to the airlight values. These data and smoothness costs build up complete MRFs that can be optimized using the existing inference methods, producing the estimated values of the airlight. Based on the estimated airlight, finally we compute the direct attenuation that represents the scene with enhanced visibility. Note that, in this paper, we do not intend to fully recover the scene's original colors or albedo. Our goal is to solely enhance the contrast of an input image so that the image visibility is improved.

Very recently, Fattal [2] independently developed a method that solely requires a single input image. The method uses a local window-based operation and a graphical model. However, unlike our proposed method, it attempts to separate uncorrelated fields, namely, the object shading and the particle attenuation.

The remaining of this paper is organized as follows. In Section 2, we describe the optical model of bad weather, and derive the model in term of chromaticity. In Section 3, we explicitly define the problem of visibility enhancement. In Section 4, we introduce the theoretical solutions of the problem, followed by Section 5 where we describe the detail of the solutions in practical frameworks. We show some results on real images in Section 6. Finally, in Section 7, we discuss our future work and conclude the paper.

2. Optical Model

The optical model usually used in dealing with bad weather, particularly in computer vision, is described as [1, 8, 10, 7]:

$$\mathbf{I}(x) = \mathbf{L}_\infty \rho(x) e^{-\beta d(x)} + \mathbf{L}_\infty (1 - e^{-\beta d(x)}). \quad (1)$$

The first term is the direct attenuation, and the second term is the airlight. \mathbf{I} is the image intensity. x is the 2D spatial location. \mathbf{L}_∞ is the atmospheric light, which is commonly assumed to be globally constant, thus it is indepen-

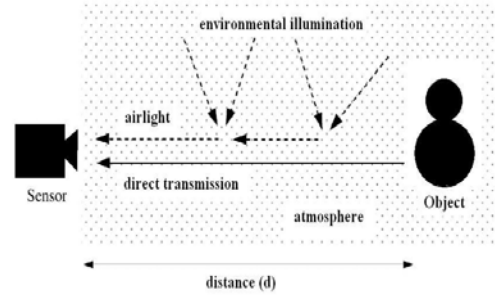


Figure 2. The pictorial description of the optical model

dent from location x . ρ is the reflectance of an object in the image. β is the atmospheric attenuation coefficient. d is the distance between an object in the image and the observer. β in the equation is assumed to be constant for different wavelengths. This assumption is common in many methods dealing with particles that the size is larger compared with the wavelength of light [5], such as, fog, haze, aerosol, etc. Moreover, β is constant for different spatial locations in the input image [7, 6]. Note that, \mathbf{I} , \mathbf{L}_∞ , ρ in the equation are color vector (rgb), while the remaining variables are scalar. Eq. (1) is in principle based on the Lambert-Beer law for transparent objects, which states that light travels through a material will be absorbed or attenuated exponentially. Figure 2 shows the pictorial description of the model. In this paper, bad weather is associated with haze, mist, fog, aerosol, etc, however it is also can be extended further to rain or snow, as long as the optical model can approximately represent the real physical world.

Chromaticity In our method, we intend to use chromaticity to describe Eq.(1), and thus define image chromaticity as follows:

$$\sigma_c = \frac{I_c}{I_r + I_g + I_b} \quad (2)$$

where index c represents the color channel (which can be either r or g or b), and this makes I_c become one of the elements of \mathbf{I} .

If we assume that the object is infinitely distant ($d = \infty$), according to Eq.(1) the image chromaticity will depend only on the atmospheric light (\mathbf{L}_∞), since $e^{-\beta d} = 0$. We call this "light chromaticity", which has definition derived from Eq.(2):

$$\alpha_c = \frac{L_{\infty c}}{L_{\infty r} + L_{\infty g} + L_{\infty b}} \quad (3)$$

Accordingly if we assume that there is no effect of scattering particles ($e^{-\beta d} = 1$), implying the absence of the airlight, then the image chromaticity will depend solely on the direct attenuation. We call this chromaticity "object chromaticity". By deriving from Eq.(2) and (1) we can write:

$$\gamma_c = \frac{L_{\infty c} \rho_c}{L_{\infty r} \rho_r + L_{\infty g} \rho_g + L_{\infty b} \rho_b} \quad (4)$$

Therefore, by using Eq.(3,4), we can rewrite Eq. (1) in terms of chromaticity:

$$\mathbf{I}(x) = D(x)e^{-\beta d(x)}\gamma(x) + A(x)\alpha \quad (5)$$

where:

$$D(x) = L_{\infty r} \rho_r(x) + L_{\infty g} \rho_g(x) + L_{\infty b} \rho_b(x) \quad (6)$$

$$A(x) = (L_{\infty r} + L_{\infty g} + L_{\infty b})(1 - e^{-\beta d(x)}) \quad (7)$$

D and A are both scalar values, while γ and α are normalized color vectors. From their chromaticity definitions, we can state $[\sum \sigma_c = \sigma_r + \sigma_g + \sigma_b = 1]$, $[\sum \gamma_c = \gamma_r + \gamma_g + \gamma_b = 1]$, and $[\sum \alpha_c = \alpha_r + \alpha_g + \alpha_b = 1]$.

Atmospheric Light and Light Chromaticity In many situations of bad weather, particularly in daylight where the sky is usually overcast, we can ignore the presence of the sunlight, and assume that the atmospheric light (\mathbf{L}_∞) is globally constant. According to Eq.(1), this global value of \mathbf{L}_∞ can be obtained from pixels that have the highest intensity in the input image. Since these pixels represent an object at infinite distant ($d = \infty$), assuming that the sky can be seen in the image and the image has no saturated pixels. Consequently, having the value of \mathbf{L}_∞ enables us to obtain the value of the light chromaticity (α), by plugging the value of \mathbf{L}_∞ into Eq.(3).

White Atmospheric Light By utilizing the light chromaticity (α), we can transform the color of the atmospheric light of the input image into white color, simply by dividing every color channel of the image intensity in Eq. (5) by the corresponding α_c :

$$I'_c(x) = I_c(x)/\alpha_c \quad (8)$$

$$I'_c(x) = D(x)e^{-\beta d(x)} \frac{\gamma_c(x)}{\alpha_c(x)} + A(x) \quad (9)$$

$$= D(x)e^{-\beta d(x)}\gamma'_c(x) + A(x) \quad (10)$$

where γ'_c is the normalized object chromaticity. I'_c is the normalized input image that the airlight color is white.

The last equation can be written in term of color vectors:

$$\mathbf{I}'(x) = D(x)\gamma'(x)e^{-\beta d(x)} + A(x) \begin{bmatrix} 1 \\ 1 \\ 1 \end{bmatrix} \quad (11)$$

where \mathbf{I}' and γ' are color vectors, and the remaining variables are scalar. Figure 3 shows the result of the normalization, where to be displayable (i.e. the intensity ranges from 0 to 255) we divide the two sides of the last equation with a scalar value. In this paper we divide by three. The last operation does not change the correlation described in Eq.(11).



Figure 3. Left: Input image. Right: the result of normalizing the environmental light.

3. Problem Definition

Considering Eq.(11) and assuming that we have the values of $\mathbf{I}'(x)$ and \mathbf{L}_∞ , the goal of this paper is therefore to estimate the values of $D(x)\gamma'(x)$ across the image. These values represent an image that is not affected by scattering or absorption.

Through the Airlight The problem of estimating $D\gamma'$ is in fact equivalent to estimating A . We can compute $D\gamma'$ from A using the following steps: first, based on Eq.(7),

$$e^{-\beta d(x)} = \frac{\sum_c L_{\infty c} - A(x)}{\sum_c L_{\infty c}} \quad (12)$$

where $\sum_c L_{\infty c} = L_{\infty r} + L_{\infty g} + L_{\infty b}$. Second, based on Eq.(11):

$$D(x)\gamma'(x) = \left(\mathbf{I}'(x) - A(x) \begin{bmatrix} 1 \\ 1 \\ 1 \end{bmatrix} \right) e^{\beta d(x)} \quad (13)$$

Consequently, instead of directly estimating $D\gamma'$, we can first estimate A , which is considerably easier to compute, since it is independent from the object reflectance (ρ), and is solely dependent on the depth, d (recall that we have assumed that β and \mathbf{L}_∞ are globally constant).

4. The Solution of Using a Single Image

The problem described in Sect. 2 is a totally ill-posed problem: the number of known variables in Eq.(11) is less than the number of unknown variables. However, there are some clues or observations that can be considered:

1. The output image, $D\gamma'$ must have better contrast compared to the input image, \mathbf{I} .
2. The variation of the values of A is dependent solely on the depth of the objects, d , implying that objects with the same depth will have the same value of A , regardless their reflectance (ρ). Thus, the values of A for neighboring pixels tend to be the same. Moreover, in many situations A changes smoothly across small local

areas. Exception is for pixels at depth discontinuities, whose number is relatively small.

Aside from the two main observations above, we can also consider that:

3. The input images that are plagued by bad weather are normally taken from outdoor natural scenes. Therefore, the correct values of $D\gamma'$ must follow the characteristics of clear-day natural images.

4.1. Maximizing Contrast

For the first clue, we quantitatively define image contrast in association with the number of edges, which can be written formally as:

$$C_{edges}(\mathbf{I}) = \sum_{x,c} |\nabla I_c(x)| \quad (14)$$

where ∇ is the differential operator over x -axis and y -axis. This equation implies that an image with more contrast produces a larger number of edges. In other words, clear-day images have a larger number of edges than those affected by bad weather: $C_{edges}(D\gamma') > C_{edges}(\mathbf{I}')$.

From Sect. 2 we know that the values of $D\gamma'$ can be obtained from A that is according to Eq.(7): $0 \leq A(x) \leq \sum_c L_{\infty c}(x)$. Therefore, if we have a small image patch, \mathbf{p} , that contains objects with the same depth and affected by bad weather, then there is a scalar value A , which can give the correct $D\gamma'$, where $D\gamma'$ must follow these constraints:

$$C_{edges}(D\gamma') > C_{edges}(\mathbf{p}) \quad (15)$$

$$0 \leq D\gamma'_c \leq L_{\infty c} \quad (16)$$

The second constraint is the direct consequence of Eq.(4,6), since $0 \leq \rho_c \leq 1$.

Figure 4 shows a natural image in a clear day and the artificial fog on the image that the airlight (A) is set constant across the image. We crop the artificial-fog image to have a small-squared patch (the red box), compute $C_{edges}(D\gamma')$ from all values of A , and plot the correlation of the two in Figure 5. As can be observed in the figure, the value of $C_{edges}(D\gamma')$ increases along with the increase of A and declines after reaching a certain peak. This rapid decline is mainly caused by imposing the second constraint (Eq.(16)).

We argue that the correlation prevails for every image patch taken from any kind of scenes plagued by bad weather, as long as the image patch has textures in it, implying that $C_{edges}(D\gamma') > 0$. The proof is as follows. Regarding Eq.(14,13,12), we can write:

$$\begin{aligned} C_{edges}(D\gamma') &= \sum_{x,c} |(I'_{x,c} - A)e^{\beta d} - (I'_{x-1,c} - A)e^{\beta d}| \\ &= e^{\beta d} \sum_{x,c} |(I'_{x,c} - I'_{x-1,c})| \\ &= \frac{\sum_c L_{\infty c}}{\sum_c L_{\infty c} - A} \sum_{x,c} |(I'_{x,c} - I'_{x-1,c})| \end{aligned}$$



Figure 4. Left: a natural image. Right: synthetic fog of the left image, where A is set constant globally (=153 after the division).

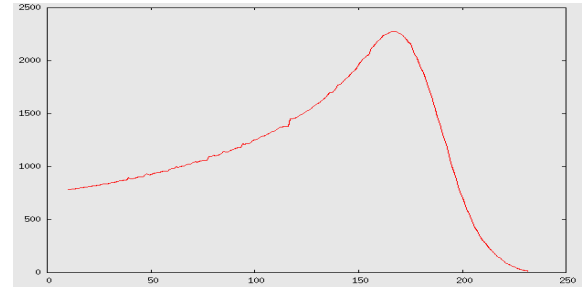


Figure 5. The distribution of the number of edges (of the region in the red rectangle) with respect to A . y-axis is $C_{edges}([D\gamma']_x^*)$ and x-axis is A . The peak is around $A = 167$.

since L_{∞} is constant and $\sum_{x,c} |(I'_{x,c} - I'_{x-1,c})|$ has the same value for the same image patch, then $C_{edges}(D\gamma')$ will be proportional to A . This explains the increase in Figure 5. However, following the second constraint in Eq.(16) we set $D\gamma'_c = 0$ if $D\gamma'_c > L_{\infty c}$, therefore $C_{edges}(D\gamma')$ will decline regardless the increase of A . Note that, d is independent from x , since we assume that A is constant across the patch.

In our framework to enhance visibility, we use $C_{edges}(D\gamma')$ as our cost function. While the largest number of $C_{edges}(D\gamma')$ does not always represent the actual value of A , it represents the enhanced visibility of the input image. As mentioned in the introduction, in this paper we do not intend to recover the original color or reflectance of the images in clear days. Our main purpose is to enhance the visibility of scenes in bad weather, with some degree of accuracy on the scene's colors.

4.2. Airlight Smoothness Constraint

According to the second clue, the changes of A across the image tend to be smooth for the majority of the pixels. This motivates us to model the airlight (A) using Markov random fields (MRFs). We write the potential function of

MRFs as:

$$E(\{A_x\}|\mathbf{p}_x) = \sum_x \phi(\mathbf{p}_x|A_x) + \eta \sum_{x,y \in N_x} \psi(A_x, A_y) \quad (17)$$

where \mathbf{p}_x is a small patch centered at location x , which is assumed to have a constant value of A_x (where $A_x \equiv A(x)$). η is the strength of the smoothness term, and N_x represents the neighboring pixels of x . We define the first term, which is the data term as:

$$\phi(\mathbf{p}_x|A_x) = \frac{C_{edges}([D\gamma']_x^*)}{m} \quad (18)$$

where $[D\gamma']_x^*$ is obtained by plugging every value of A_x into Eq.(12,13). m is a constant to normalize C_{edges} , so that $0 \leq \phi(\mathbf{p}_x|A_x) \leq 1$. The value of m depends on the size of the patch \mathbf{p}_x . The second term (the smoothness term) is defined as:

$$\psi(A_x, A_y) = 1 - \frac{|A_x - A_y|}{\sum_c L_{\infty c}} \quad (19)$$

This equation encourages smoothness for neighboring A_x .

To find all values or labels of $\{A_x\}$, we have to maximize the probability distribution of $p(\{A_x\})$ described in Gibbs distribution by using the existing inference techniques, such as graph-cuts or belief-propagation.

5. Computational Methods

In this section, we further explain the detailed implementation of the framework described in Eq.(17) and discuss a few other issues for improving the results and computational time.

5.1. Algorithm

Pseudocode 5.1 shows the detailed algorithm of our method. Given an input image \mathbf{I} , in step 1, we estimate the atmospheric light, L_{∞} . This can be done by finding a small spot that has the highest intensity in image \mathbf{I} . In step 2, we compute the light chromaticity, α from L_{∞} by using Eq.(3). However, to be more accurate, we can estimate α using an existing color constancy method (e.g. [3]). Having the value of α , in step 3, we remove the illumination color of \mathbf{I} using Eq.(8), producing \mathbf{I}' . We compute the data cost for every pixel of \mathbf{I}' in step 4. The detail of the algorithm for computing the data cost is described in Pseudocode 5.2.

Pseudocode 5.2 starts with an iteration of every pixel in \mathbf{I}' . x represents 2D location of a pixel. In step 4.1, we crop an $n \times n$ patch which is centered at a location x . n must be small enough to make the assumption that the airlight in the patch is uniform valid, yet not so small that we could possibly lose the textures or edges information. The patch size could be 5×5 or 7×7 , depending on the size and scale of the input image. In step 4.2 and 4.2.1, for every possible value of A , which each of them we call A^* , we compute the direct attenuation for the patch, $[D\gamma']_x^*$, using Eq.(13). Then, in step 4.2.2, we compute the data cost using Eq.(18).

After all of the iterations finish, the function will return the data cost, $\phi(\mathbf{p}_x|A_x)$ for all pixels, where for each pixel, $\phi(\mathbf{p}_x|A_x)$ is a vector with $(\sum_c L_{\infty c} - k)$ dimensions. For clarity, we explain the constant k later in this section.

Algorithm 5.1: VISIBILITYENHANCEMENT(\mathbf{I})

comment: \mathbf{I} is the input image

- (1) Estimate L_{∞}
- (2) Compute α from L_{∞}
- (3) Remove the illumination color of \mathbf{I}
- (4) Compute the data term $\phi(\mathbf{p}_x|A_x)$ from \mathbf{I}'
- (5) Compute the smoothness term $\psi(A_x, A_y)$
- (6) Do the inference, which yields the airlight, A
- (7) Compute the direct attenuation, $D\gamma'$, from A
- return** ($D\gamma'$)

Algorithm 5.2: DATACOST(\mathbf{I}' , $\sum_c L_{\infty c}$)

```

for  $x \leftarrow 0$  to  $\text{sizeof}(\mathbf{I}') - 1$ 
{
  (4.1) Crop an  $n \times n$  patch,  $\mathbf{p}_x$ , from  $\mathbf{I}'$  centered at  $x$ 
  (4.2) for  $A^* \leftarrow 0$  to  $\sum_c L_{\infty c} - k$ 
  {
    (4.2.1) Compute  $[D\gamma']_x^*$  from  $A^*$  and  $\mathbf{p}_x$ 
    (4.2.2) Compute  $\phi(\mathbf{p}_x|A_x^*) = \frac{C_{edges}([D\gamma']_x^*)}{m}$ 
  }
  return ( $\phi(\mathbf{p}_x|A_x)$  for all pixels)
}

```

After computing the data cost, in step 5 of Pseudocode 5.1, we compute the smoothness cost using Eq.(19). By obtaining both data cost and smoothness cost, we now have a complete graph in term of Markov random fields. In Step 6, to do the inference in MRFs with number of labels equals to $(\sum_c L_{\infty c} - k)$, we use the graph-cut algorithm with multiple labels (i.e. [12]) or belief propagation. In step 7, we finally compute the direct attenuation for the whole image from the estimated airlight using Eq.(13). Figure 6, show the results of the airlight, A , and the corresponding $D\gamma'$.

Up to this point, there are two variables that are not yet discussed: k (in step 2 of Pseudocode 5.2) and the value of η in Eq.(17). In Section 4.1., we have mentioned that $0 \leq A \leq \sum_c L_{\infty c}$, thus the iteration in step 2 (of 5.2) should be from 0 to $\sum_c L_{\infty c}$. However we know that, $A = \sum_c L_{\infty c}$ only when the object is infinitely distant, and in fact, most objects are not at infinity, except for the sky itself. Therefore A must be smaller than $\sum_c L_{\infty c}$ that we write mathematically as $0 \leq A \leq \sum_c L_{\infty c} - k$, where in our experiments, we set $k = 20$.

To determine η we can empirically learn from a database of foggy images and their corresponding clear-day images. We examine η by comparing images that have been enhanced using various η with their corresponding clear day images, and choose the best η that gives considerably good results for the majority of the images.

Gray Images For gray images, the algorithm is exactly the same, except that we skip step 3 (of Pseudocode 5.1), meaning that we do not estimate α and do not remove the illumination color. Figure 7 show the result of enhancing visibility for a gray image.



Figure 6. Top: the airlight. Bottom: the direct attenuation.

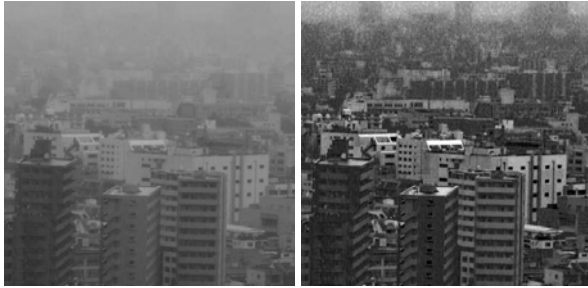


Figure 7. Left: a gray input image. Right: the enhanced image.

5.2. Label Candidates and Initialization

Graph-cuts and belief propagation are currently the most efficient techniques to optimize the cost function of MRFs, unfortunately they still require a considerable amount of

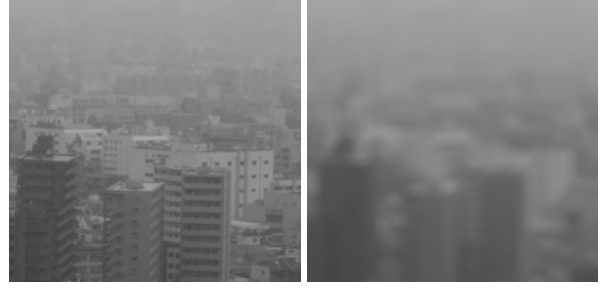


Figure 8. Left: the values of Y. Right: the blurred Y-image.

computational time, particularly when the size of the input image and the number of labels are large. To speed up the inference process, we consider two techniques: first, by reducing the number of labels (the dimension of the data cost), and second, by providing initial values for the airlight.

In Pseudocode 5.2, the number of labels (the dimension of the data cost, $\phi(\mathbf{p}_x|A_x)$) is fixed, i.e., $(\sum_c L_{\infty c} - k)$, however we know that not all of these labels are actually used. For instance, if we have the largest $C_{edge}([D\gamma']^*)$ at $A^* = 200$, then it is not possible that the actual A for the patch is equal to 0 or even 50. Therefore, we reduce the number of the labels by choosing the n^{th} -largest data cost and its corresponding A^* , where in our experiments we defined $n = 20$.

For obtaining the initial values of the airlight (A), we approximately estimate it through the Y of YIQ color model, which is defined as:

$$Y = 0.257\mathbf{I}'_r + 0.504\mathbf{I}'_g + 0.098\mathbf{I}'_b \quad (20)$$

We blur the image that is produced by the values of Y and use this blurred image as the initial values of A. Figure 8 show the values Y, and the blurred Y (the initial airlight).

6. Experimental Results

To demonstrate the effectiveness of our method, we used real images of outdoor scenes in our experiments. We did not apply radiometric calibration to our experiments, however we consider that a camera with gamma correction turned off will improve the results, particularly for obtaining the appropriate colors with respect to the actual colors in clear days. The computational time for 600×400 images, using double processors of Pentium 4 and 1 GB memory, approximately five to seven minutes (applying graph-cuts with multiple labels).

Top of Figure 9 shows a road scene partially covered by haze. The middle and the bottom of the figure show the direct attenuation image and the airlight. In the direct attenuation image, one can observe that a yellow car which is far away from the camera becomes visible. Figure 10, which was obtained from the internet, shows an outdoor scene plagued by fog. The middle and bottom of the figure show the direct attenuation and the airlight. Figure 11 shows the input image of rainy weather, the estimated direct



Figure 9. *Top: input image. Middle: the direct attenuation. Bottom: the airlight.*

attenuation, the ground truth, and the estimated airlight. We consider the image taken in clear weather to be the ground truth.

The inference for the last result was done by using Iterated Conditional Modes (ICM) employing the blurred Y-image as the initial values. Although ICM cannot guarantee the global optimum, the result shows that the visibility is considerably improved. This is due to the effectiveness of our cost function and the initial values.

7. Future Work and Conclusion

For future work, we intend to concentrate on the current constraints of our method. First is the halos at depth discontinuities. One can observe, for instance in Figure 9,



Figure 10. *Top: input image. Middle: the direct attenuation. Bottom: the airlight.*

there are some small halos surrounding the trees in the image. We suspect that it is due to the patch-based operation we use; and, this problem should be straightforward to solve if we know the depth discontinuities of the scenes (which, in the input image, are obscured by the atmospheric particles). The second constraint is that, since we optimize the data cost function and do not know the actual values of A , the outputs tend to have larger saturation values (of hue-saturation-intensity) than those in the actual clear-day images. To overcome this, we intend to incorporate the observation 3 in Section 4, namely that the outputs must follow the characteristics of natural images of clear-day scenes. We hypothesize that these characteristics can be learned statistically. Finally, we also intend to apply the proposed method



Figure 11. Top: input image. Second from top: the direct attenuation. Third from the top: the ground truth. Bottom: the airlight. Note that, we increase the intensity of the direct attenuation, since the input image is considerably darker than the ground truth.

to improve under-water visibility [9] or other turbid media that have the same optical model.

As a conclusion, we have introduced a method that is solely based on single images, without requiring the geometrical structure of the world nor any user interactions. We believe that many applications, such as outdoor surveillance systems, intelligent vehicle systems, remote sensing systems, graphics editors, etc, could benefit from our proposed method.

Acknowledgements

Thanks to Richard Hartley and Sing Bing Kang for the valuable discussions. Also, to Lars Petersson and Niklas Pettersson for encouraging me to tackle the problem. This research was conducted when I was part of Smart Car Project in NICTA/The Australian National University. NICTA is funded by the Australian Government as represented by the Department of Broadband, Communications and the Digital Economy and the Australian Research Council through the ICT Centre of Excellence program.

References

- [1] F. Cozman and E. Krotkov. Depth from scattering. In *Proceedings of the 1997 Conference on Computer Vision and Pattern Recognition*, vol. 31, pp. 801–806., 1997. 1, 2
- [2] R. Fattal. Single image dehazing. to appear in *SIGGRAPH*, 2008. 2
- [3] A. Gijsejij and T. Gevers. Color constancy using natural image statistics. in *proceeding of IEEE CVPR*, 2007. 5
- [4] N. Hautiere, J. Tarel, and D. Aubert. Toward fog-free in-vehicle vision systems through contrast restoration. *CVPR*, 2007. 1
- [5] E. McCartney. *Optics of the atmosphere: Scattering by molecules and particles*. John Wiley and Son, 1975. 2
- [6] S. Narasimhan and S. Nayar. Interactive deweathering of an image using physical models. *IEEE Workshop on Color and Photometric Method in Computer Vision*, 2003. 1, 2
- [7] S. G. Narasimhan and S. K. Nayar. Contrast restoration of weather degraded images. *IEEE PAMI*, 25(6), June 2003. 1, 2
- [8] S. K. Nayar and S. G. Narasimhan. Vision in bad weather. In *ICCV(2)*, pages 820–827, 1999. 1, 2
- [9] Y. Schechner and N. Napel. Clear underwater vision. *CVPR*, 2004. 8
- [10] Y. Y. Schechner, S. G. Narasimhan, and S. K. Nayar. Instant dehazing of images using polarization. 1:325–332, 2001. 1, 2
- [11] S. Shwartz, E. Namer, and Y. Schechner. Blind haze separation. *CVPR*, 2006. 1
- [12] R. Szeliski, R. Zabih, D. Scharstein, O. Veksler, V. Kolmogorov, A. Agarwala, M. Tappen, , and C. Rother. A comparative study of energy minimization methods for markov random fields. in *proceeding of ECCV*, 2006. 5